

N4-acetylation of cytidine in mRNA plays essential roles in plants

Wenlei Wang ^{1,†} Huijie Liu ^{1,†} Feifei Wang ¹ Xiaoye Liu ² Yu Sun ¹ Jie Zhao ¹
Changhua Zhu ¹ Lijun Gan ¹ Jinping Yu ³ Claus-Peter Witte ⁴ and Mingjia Chen ^{1,*}

- 1 College of Life Sciences, Nanjing Agricultural University, Nanjing 210095, P.R. China
- 2 Department of Criminal Science and Technology, Nanjing Forest Police College, Nanjing 210023, P.R. China
- 3 Jiangsu Key Laboratory for the Research and Utilization of Plant Resources, Institute of Botany, Jiangsu Province and Chinese Academy of Sciences (Nanjing Botanical Garden Mem. Sun Yat-Sen), Nanjing 210014, P.R. China
- 4 Department of Molecular Nutrition and Biochemistry of Plants, Institute of Plant Nutrition, Leibniz University Hannover, Hannover 30419, Germany

*Author for correspondence: mjchen@njau.edu.cn

[†]Joint First Authors.

The author responsible for distribution of materials integral to the findings presented in this article in accordance with the policy described in the Instructions for Authors (<https://academic.oup.com/plcell/pages/General-Instructions>) is: Mingjia Chen (mjchen@njau.edu.cn).

Abstract

The biological function of RNA can be modulated by base modifications. Here, we unveiled the occurrence of N4-acetylation of cytidine in plant RNA, including mRNA, by employing LC-MS/MS and acRIP-seq. We identified 325 acetylated transcripts from the leaves of 4-week-old *Arabidopsis* (*Arabidopsis thaliana*) plants and determined that 2 partially redundant N-ACETYLTRANSFERASES FOR CYTIDINE IN RNA (ACYR1 and ACYR2), which are homologous to mammalian NAT10, are required for acetylating RNA in vivo. A double-null mutant was embryo lethal, while eliminating 3 of the 4 ACYR alleles led to defects in leaf development. These phenotypes could be traced back to the reduced acetylation and concomitant destabilization of the transcript of *TOUGH*, which is required for miRNA processing. These findings indicate that N4-acetylation of cytidine is a modulator of RNA function with a critical role in plant development and likely many other processes.

Introduction

Over 150 chemical nucleoside modifications have been discovered in different RNA species of eukaryotes. Most are present in noncoding RNAs, such as transfer RNA and ribosomal RNA, but mRNA also contains modified bases such as N6-methyladenosine (m⁶A), N1-methyladenosine, N7-methylguanosine, 5-methylcytidine, N4-acetylcytidine (ac⁴C), and pseudouridine (Frye et al. 2016; Frye et al. 2018; McCown et al. 2020). These mRNA modifications are installed by “writer” proteins on pre-mRNA in the nucleus, and some modifications can be dynamically removed by “eraser” proteins. The mRNA modifications influence gene expression by regulating pre-mRNA splicing, mRNA structure, transport, stability, and translation efficiency (Shen

et al. 2019; Wiener and Schwartz 2021). Often “reader” proteins are involved in decoding the modification signature. Among the different types of mRNA modifications, ac⁴C is the only acetylation modification (Fig. 1A) (Arango et al. 2018). ac⁴C was recently identified in mammalian mRNA (Arango et al. 2018), where it is introduced by the ac⁴C writer N-ACETYLTRANSFERASE 10 (NAT10). Acetylation of mRNA not only occurs in mammals but also has been reported in archaea (Sas-Chen et al. 2020). RNA immunoprecipitation with ac⁴C antibodies followed by deep sequencing (acRIP-seq) identified thousands of ac⁴C sites in the mRNA of HeLa cells, with most mapping near the translation start sites within the coding sequences, promoting mRNA stability and translation initiation in this human cell line (Arango et al.

IN A NUTSHELL

Background: Eukaryotic mRNA harbors more than 10 different chemical modifications, most of which are involved in many cellular activities such as RNA processing, RNA degradation, and translation. These chemical modifications are installed by “writer” proteins on pre-mRNA. N⁴-acetylcytidine (ac⁴C), the only known type of RNA acetylation modification, has recently been reported in mammalian mRNA. This modification is introduced by a single-copy acetyltransferase NAT10 and promotes translation efficiency.

Question: Does ac⁴C modification widely exist in plant mRNA and what are the biological functions of this chemical modification?

Findings: Our data demonstrate the wide occurrence of ac⁴C modification on RNAs from several vascular plants. Employing acRIP-seq, we mapped the distribution of ac⁴C modifications in *Arabidopsis thaliana*. We also show that *Arabidopsis* RNAs are acetylated by N-ACETYLTRANSFERASES FOR CYTIDINE IN RNA 1 (ACYR1) and ACYR2, which are homologs of human NAT10. A double-null mutation is embryo lethal, while abolishing 3 of the 4 ACYR alleles leads to defects in vegetative development. This phenotypic alteration is caused by the accelerated degradation of *TOUGH* transcript, a component of miRNA biogenesis, when its ac⁴C levels are reduced.

Next steps: The identification and characterization of ac⁴C in plant RNA give rise to the field of RNA modification and open up many research questions. Are any other proteins involved in ac⁴C formation and/or removal? Does ac⁴C modification participate in other developmental processes and/or environmental stimuli? What are the molecular mechanisms of ac⁴C modification regulating the target transcripts?

2022). In plants, acetylation of cytidine within RNA, especially mRNA, remains poorly understood.

MicroRNAs (miRNAs) are small endogenous regulatory RNAs that are ~21 nt in length and affect the translation or stability of target mRNAs (Jones-Rhoades et al. 2006; Voinnet 2009; Dolata et al. 2018). Mature miRNAs are derived from long primary transcripts that are produced by RNA polymerase II and further processed by the dicing complex, which in *Arabidopsis* (*Arabidopsis thaliana*) contains DICER-LIKE1 (DCL1), HYPONASTIC LEAVES1 (HYL1), and SERRATE (SE) as the core proteins (Yu et al. 2017). Several other proteins, including TOUGH (TGH), are associated with the dicing complex and co-regulate the production of miRNAs in response to developmental and environmental signals (Ren et al. 2012; Samad et al. 2017; Dolata et al. 2018). The TGH protein consists of 2 conserved functional domains with a role in RNA binding and RNA processing (Calderon-Villalobos et al. 2005). In *Arabidopsis*, loss of TGH function suppresses the activity of DCL1 and the interaction between pri-miRNA and HYL1. This prevents the accumulation of mature miRNAs (Ren et al. 2012), resulting in severe defects in leaf development (Calderon-Villalobos et al. 2005).

Here, we utilized mass spectrometry and transcriptome-wide approaches to investigate the occurrence, distribution, and function of ac⁴C in plant mRNAs. acRIP-seq data revealed that ac⁴C modifications are widespread within the *Arabidopsis* transcriptome. In protein-coding transcripts, they are enriched in the coding sequences. We identified 2 cytidine-N-acetylases required for acetylating *Arabidopsis* RNA in vivo and investigated the molecular and phenotypic consequences of altering cytidine-N-acetylation by genetic manipulation. While total loss of ac⁴C was lethal, reduced

N-acetylation of cytidine compromised rosette development. A correlation analysis of acetylation states and transcript abundances provided a plausible connection between reduced transcript acetylation and defects in the miRNA processing machinery. As a result, *TGH*, which is involved in miRNA biogenesis, is deregulated, providing a functional link to the phenotypic consequences of reduced cytidine acetylation.

Results

Plant mRNAs are acetylated on cytidines

To investigate whether ac⁴C is present in plant mRNAs, we isolated mRNA from total RNA of 2-week-old *Arabidopsis* seedlings using 2 rounds of oligo dT purification. The mRNA purity was assessed using a bioanalyzer (Fig. 1B) and by detecting the level of 18S rRNA contamination relative to the *ACTIN2* transcript level in the mRNA using RT-qPCR assays (Supplemental Fig. S1). We determined the amount of ac⁴C in mRNA and total RNA by completely RNA digestion to nucleosides followed by liquid chromatography coupled to quadrupole mass spectrometry (LC-MS/MS). For both total RNA and mRNA, we observed peaks in the respective analyses matching the retention time of the N⁴-acetylcytidine standard (2.29 min) with similar MS/MS profiles showing mass transitions of *m/z* 286.3 to 112.0 and more prominently to 153.9 (Supplemental Fig. S2). This demonstrates that ac⁴C was present in these RNA preparations. A quantitative evaluation revealed that approximately 29-fold more ac⁴C was present in total RNA (0.115 ± 0.005% ac⁴C relative to unmodified C) than in the mRNA preparation (0.004 ± 0.0017%, Fig. 1C). We confirmed the

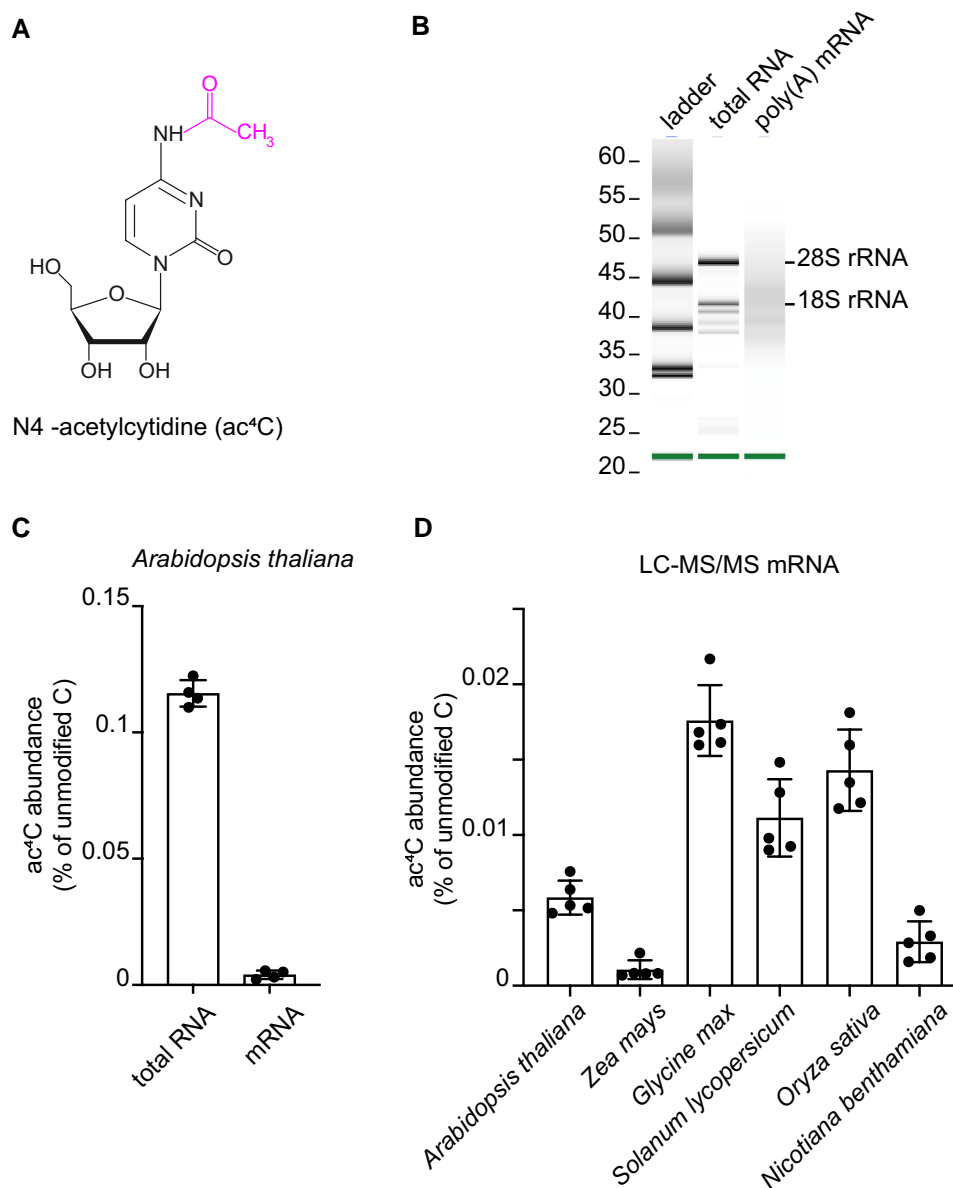


Figure 1. Presence of ac⁴C in plant RNAs. **A)** Chemical structure of N4-acetylcytidine. **B)** The integrity of the purified RNA samples and the efficient removal of rRNA from mRNA were analyzed using Bioanalyzer 2100. **C)** LC-MS/MS analysis of the ac⁴C/C ratio in total RNA and mRNA of 2-week-old seedlings. Error bars are SD ($n = 4$ biological replicates; biological replicates are parallel measurements of biological distinct samples). **D)** LC-MS/MS analysis of the ac⁴C/C ratio in mRNA of leaves from 3-week-old seedlings of different plant species. Error bars are SD ($n = 5$ biological replicates; biological replicates are parallel measurements of biological distinct samples).

purity of the mRNA by showing that 3-methyluridine (m³U), a modification that only occurs in rRNA (McCown et al. 2020), was not detectable in our mRNA preparation (Supplemental Fig. S3). Furthermore, given that the abundance of 18S rRNA was reduced more than 1,000-fold in the mRNA sample versus total RNA (Supplemental Fig. S1) but that there was only 29-fold less ac⁴C in the mRNA (Fig. 1C), the detected ac⁴C in the mRNA could not have resulted from contamination with noncoding RNAs. Taken together, these data demonstrate that N4-acetylation of cytidine is a bona fide mRNA modification in *Arabidopsis*.

We also investigated if ac⁴C is present in leaf mRNA from several other plant species. The modification was detected in all species examined, i.e. maize (*Zea mays*, $0.0011 \pm 0.0006\%$ ac⁴C relative to unmodified C), soybean (*Glycine max*, $0.0176 \pm 0.0024\%$), tomato (*Solanum lycopersicum*, $0.0111 \pm 0.0026\%$), rice (*Oryza sativa*, $0.0143 \pm 0.0027\%$), and *Nicotiana benthamiana* ($0.00292 \pm 0.0014\%$) (Fig. 1D). Notably, the ac⁴C abundance in different species was not correlated with their genome sizes. These data demonstrate that the ac⁴C modification of mRNA occurs widely in plants.

Arabidopsis possesses 2 cytidine N-acetyltransferases

In mammalian cells, the acetyltransferase NAT10 installs ac⁴C on noncoding RNA (ncRNA) and mRNA (Arango et al. 2018). We used the protein sequence of human NAT10 as a BLAST query against predicted plant proteomes deposited at Phytozome (<https://phytozome-next.jgi.doe.gov/>), resulting in the identification of NAT10 homologs from 46 plant species (Supplemental Data Set 1). For plants, we suggest naming these enzymes N-ACETYLTRANSFERASEs FOR CYTIDINE IN RNA (ACYR). In addition, we searched the Concise Protein Database at the National Center for Biotechnology Information, which contains data from fully sequenced genomes, using human NAT10 as query and selected sequences from 13 nonplant organisms (Supplemental Data Set 1). Notably, NAT10/ACYR is a single-copy gene in all selected nonplant species and also in many plant species. However, the genomes of Cruciferae encode 2 ACYR proteins that are also phylogenetically well separated (Fig. 2 and Supplemental Data Set 1), indicating that they may have distinct functional roles. In *Arabidopsis*, we named these 2 proteins ACYR1 and ACYR2, encoded at the loci At1g10490 and At3g57940, respectively. Despite the phylogenetic separation, ACYR1 and ACYR2 are quite similar, with over 84% identical amino acids in their protein sequences (Supplemental Fig. S4). RT-qPCR analysis revealed that both genes are expressed in all tissues investigated, with slightly higher expression of ACYR1 in the apical meristem, rosette leaves, and flowers (Fig. 3A), which is in agreement with publicly available transcriptome data (*Arabidopsis* eFP browser: <https://bar.utoronto.ca/efp/cgi-bin/efpWeb.cgi>). Given the sequence similarity, the overlapping expression domains, and the finding that most plants just have 1 ACYR gene, it appears possible that the functions of ACYR1 and ACYR2 are at least partially redundant.

Subcellular localization analysis revealed that N-terminal yellow fluorescent protein (YFP) fusions with ACYR1 or ACYR2 predominantly accumulated in the nucleus and were enriched in a sub-nuclear localization, possibly the nucleolus (Fig. 3B), which is in line with the notion that most RNA modifications are installed before nuclear export.

Arabidopsis ACYRs are required for gametophytic transmission and vegetative growth

We isolated 2 independent homozygous T-DNA insertion mutants for each gene. RT-qPCR and nonquantitative RT-PCR analyses using primers flanking the insertion site showed that intact mRNA was absent in both homozygous mutants (*acyr1* and *acyr2*) and that the abundance of the defective mRNA was strongly reduced compared to the wild type (Fig. 4 and Supplemental Fig. S5). A mutation in only 1 ACYR gene had no influence on the expression of the other gene (Fig. 4B).

We attempted to generate *acyr1 acyr2* double mutant lines by crossing *acyr1-2* and *acyr2-1*. Despite several attempts, double mutants could never be recovered.

Nonetheless, plants homozygous for the T-DNA insertion at 1 locus and heterozygous at the other (hemizygous ACYR double mutants) could be recovered (*acyr1-2/acyr1-2 acyr2-1/ACYR2* and *acyr1-2/ACYR1 acyr2-1/acyr2-1*; referred to as *acyr1 acyr2/+* and *acyr1/+ acyr2* hereafter for simplicity). The transcript levels of ACYR1 or ACYR2 were significantly lower in seedlings of both hemizygous ACYR double mutants compared to the wild type (Supplemental Fig. S6). In line with the absence of a homozygous double mutant in the progeny of the segregating populations, the segregation ratios in the progeny of self-pollinated hemizygous ACYR double mutant plants (either *acyr1 acyr2/+* or *acyr1/+ acyr2*) were abnormal. Instead of the theoretical 1:2:1 genotype ratio for the hemizygous locus, the observed ratio was closer to ~1:1:0 in the progeny of *acyr1 acyr2/+* and ~20:1:0 in the progeny of *acyr1/+ acyr2* plants. Taken together, these data indicate that ACYR1 and ACYR2 are at least partially redundant and are together essential during gametogenesis and/or embryo development. In addition, both hemizygous double mutant plants produced shorter siliques than the wild type (Fig. 5A to C and Supplemental Table S1), hinting at a problem in seed development. We observed approximately 35.8% and 50.8% aborted seeds in the siliques formed by *acyr1 acyr2/+* and *acyr1/+ acyr2* plants, respectively, compared to less than 5% in the wild type (Col-0) and the single mutants (Supplemental Table S1). These results indicate that gametophytic transmission is affected in these hemizygous ACYR double mutant plants.

To comprehensively investigate the influence of ACYR-mediated RNA acetylation on plant growth, we generated a complementation line by introducing an ACYR1-*Strep* transgene encoding a *Strep* tag fused to the C-terminus of ACYR1 into the *acyr1 acyr2/+* background and named it *acyr1 acyr2/+ ACYR1-Strep*. In this line, the transgene was expressed at a level comparable to ACYR1 in Col-0. Moreover, ACYR1-*Strep* protein accumulated in transgenic seedlings, as revealed by immunoblot analysis using an anti-*Strep* antibody (Supplemental Fig. S7).

Next, we performed phenotypic analyses of Col-0, the *acyr1* and *acyr2* single mutants, the 2 hemizygous ACYR double mutants, and the complementation line grown under long-day conditions. The *acyr1* and *acyr2* single mutants were phenotypically indistinguishable from the wild type (Fig. 5D and Supplemental Fig. S8). By contrast, both hemizygous ACYR double mutants produced significantly fewer leaves and had smaller rosettes compared to Col-0, the single mutants, and the complementation line (Fig. 5D to F). The effect became apparent starting 20 days after seed imbibition (dai) based on rosette diameter (Fig. 5F). The hemizygous ACYR double mutants produced approximately 12 to 13 rosette leaves before flowering at 39 dai, while Col-0 and the single mutants produced 17 to 18 rosette leaves under the same conditions (Fig. 5D and E). Importantly, this phenotype was complemented by the ACYR1-*Strep* transgene in the *acyr1 acyr2/+* background (Fig. 5), showing that the defects in the ACYR genes caused the phenotypic alteration.

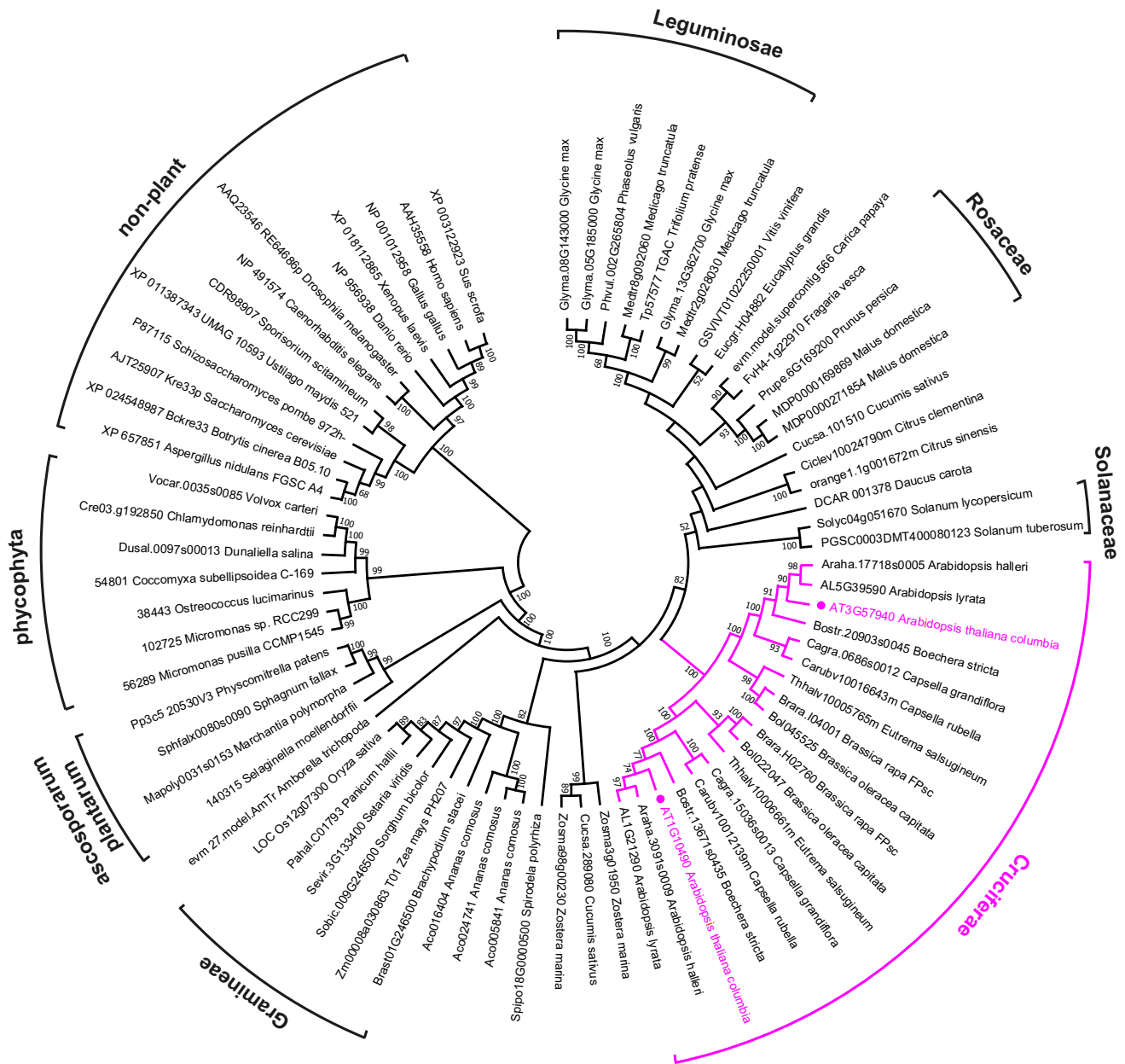


Figure 2. Sequence clades of eukaryotic NAT10/ACYR enzymes. A neighbor-joining tree was constructed with NAT10 sequences from 46 phylogenetically distant plants and 13 nonplant organisms. A total of 1,000 bootstraps were performed, and branches with bootstrap values below 50% were collapsed.

Arabidopsis RNA is acetylated by ACYRs

To explore the consequences of the loss of ACYR1 and ACYR2 on cytidine acetylation of RNA, we measured ac⁴C abundance in total RNA and mRNA from rosette leaves of 4-week-old Col-0, *acyr1*, *acyr2*, the 2 hemizygous ACYR double mutants, and the complementation line. Compared to the wild type, total RNA of *acyr1* plants contained over 3.5-fold less ac⁴C, while in *acyr2* plants, the ac⁴C abundance was approximately 1.3-fold lower (Fig. 6A). In the *acyr1 acyr2/+* line, the amount of ac⁴C was even slightly more reduced than in *acyr1*. In the mRNA, the ac⁴C/C ratios of all mutants were also smaller than that of the wild type

(Fig. 6B). Interestingly, both hemizygous ACYR double mutant lines contained markedly less ac⁴C in mRNA than the respective single mutants (Fig. 6B). Moreover, the ac⁴C/C ratios in total RNA and mRNA of the complementation line were similar to those in Col-0 (Fig. 6), indicating that the fusion protein was functional and that the observed molecular phenotype was indeed caused by the loss of ACYR1 function. These data suggest that (1) both ACYR1 and ACYR2 are required for cytidine N4-acetylation of ncRNA and mRNA in *Arabidopsis*, (2) most ac⁴C modifications are written by ACYR1, and (3) the redundancy of both writers is likely less pronounced for mRNA acetylation than for ncRNA

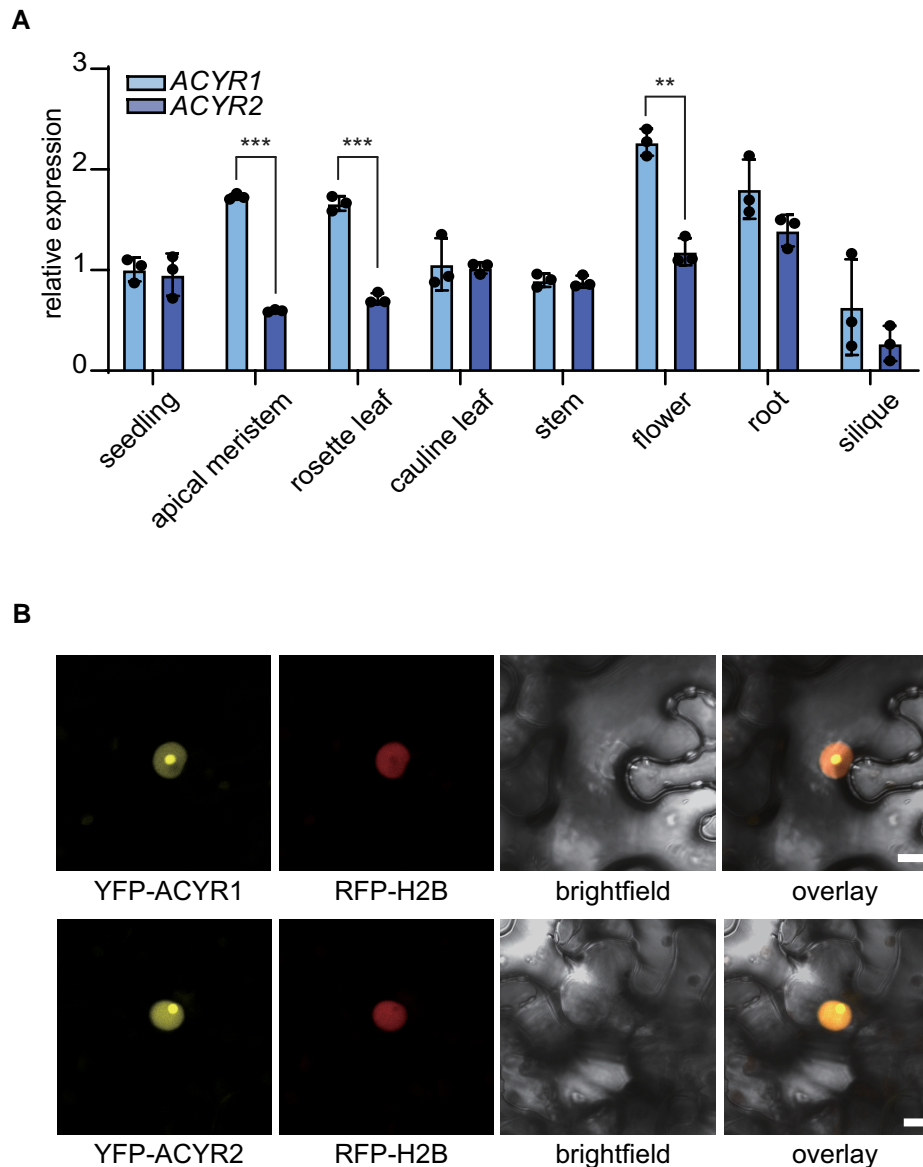


Figure 3. *ACYR1* and *ACYR2* are expressed in all tissues and localize to the nucleus. **A)** Relative expression quantified by RT-qPCR of *ACYR* genes using the primers Cp175 and Cp176 or Cp177 and Cp178 in different *Arabidopsis* tissues. Error bars are SD ($n = 3$ biological replicates; biological replicates are parallel measurements of biological distinct samples). Asterisks indicate the significant differences ($**P < 0.01$ and $***P < 0.001$, one-way ANOVA). **B)** Confocal fluorescence microscopy images of *N. benthamiana* cells from the lower leaf epidermis transiently coproducing RFP-H2B and *ACYR1* fused to an N-terminal YFP tag (YFP-*ACYR1*). Channels (from left to right): YFP, RFP, brightfield, and overlay of YFP, RFP, and brightfield. All infiltrated cells exhibited the same pattern. Bar = 10 μm . Lower panels show the results for N-terminal YFP-tagged *ACYR2*.

acetylation, i.e. there are more sites on mRNA where ac⁴C is preferentially introduced by only 1 of the enzymes. This became apparent when the gene dosage was lowered, as in the hemizygous double mutants, because the lower target affinity of either *ACYR1* for preferential *ACYR2* targets or vice versa could no longer be masked by high enzyme abundance.

Transcriptome-wide mapping of ac⁴C sites in *Arabidopsis* using acRIP-seq

To explore the impact of *ACYR* activities on the distribution of ac⁴C in RNA species, we performed acetylated RNA

immunoprecipitation and sequencing (acRIP-seq) using RNA extracted from rosette leaves of 4-week-old plants of the wild type and the 2 hemizygous *ACYR* double mutants, with 2 biological replicates per genotype. RNA was fragmented into oligonucleotides with a length of ~ 150 nucleotides (input), followed by immunoprecipitation using an anti-ac⁴C antibody. The purified RNA was used for library construction and sequencing (Fig. 7A). Adaptors and low-quality reads were removed from the raw data, and the clean reads were mapped to the *Arabidopsis* TAIR10 genome. We called ac⁴C peaks with the MACS2 algorithm (Zhang et al. 2008),

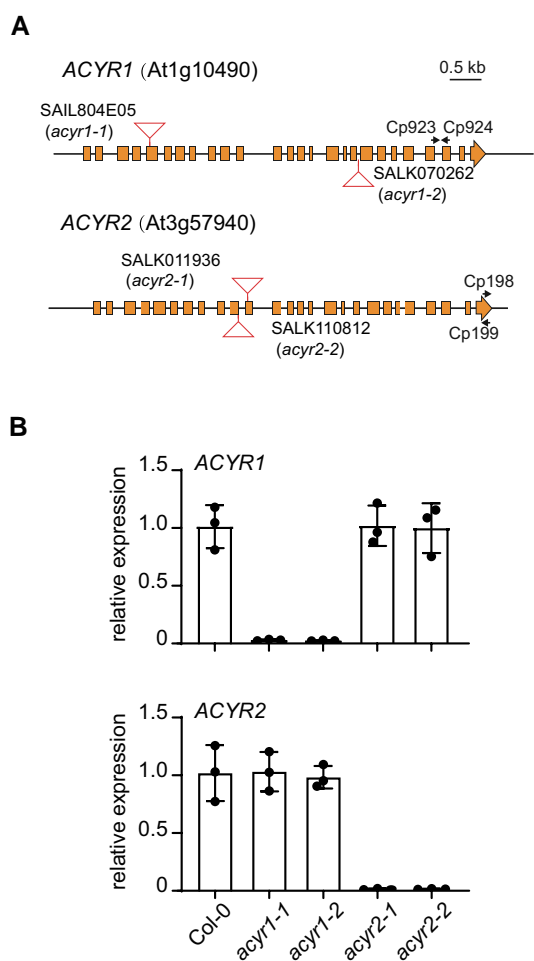


Figure 4. Characterization of plants varying in ACYR1 or ACYR2 expression. **A**) Genomic organization of the ACYR1 (At1g10490) and ACYR2 (At3g57940) loci and positions of the T-DNA insertions (triangles) in *acyr1-1* (SAIL804E05), *acyr1-2* (SALK070262), *acyr2-1* (SALK011936), and *acyr2-2* (SALK110812). Coding sequences are shown as boxes. **B**) Relative expression of ACYR1 or ACYR2 quantified by RT-qPCR using the primers Cp923 and Cp924 or Cp198 and Cp199 in wild type and single mutants of ACYR1 and ACYR2. cDNA was reverse transcribed using oligo dT. The *TIP41-like* gene was set as internal reference gene. The calculation was based on the $2^{-\Delta\Delta CT}$ method. Error bars are SD ($n = 3$ biological replicates; biological replicates are parallel measurements of biological distinct samples).

with an estimated false discovery rate (FDR) of <0.05 and an absolute fold enrichment of >1 . Correlation analysis between biological repeats confirmed that the acRIP-seq data were robust (Supplemental Fig. S9). When ac⁴C peaks were present in both biological replicates, we classified them as “confident peaks” (Supplemental Fig. S10).

In general, ac⁴C modifications were more abundant in Col-0 than in the 2 hemizygous ACYR double mutant lines in terms of the quantity of modified fragments mapping to the same genomic location (Fig. 7B), which is in agreement with the results from mass spectrometry (Fig. 6B). Also, in terms of the number of genomic locations carrying a

modification, there were more in Col-0 than the double mutants. In total, we identified 470 confident peaks for ac⁴C associated with 325 transcripts in Col-0, 329 confident peaks associated with 278 transcripts in *acyr1 acyr2/+*, and 213 confident peaks associated with 173 transcripts in *acyr1/+ acyr2* (Fig. 7C and Supplemental Data Set 2). Employing the DAVID Bioinformatics Resources (<https://david.ncifcrf.gov/>), Gene Ontology (GO) analysis revealed that the 325 ac⁴C-containing transcripts in Col-0 were enriched in transcripts related to photosynthesis and cold acclimation, indicating that ac⁴C modification in *Arabidopsis* may play an essential role in these biological processes (Supplemental Fig. S11). Compared with Col-0, 679 and 607 ac⁴C peaks differed in *acyr1 acyr2/+* and *acyr1/+ acyr2*, respectively, in terms of presence or absence in the respective genotypes (Supplemental Fig. S12). Often the same peaks were different irrespective of which mutant was compared with the wild type (in 531 cases). Of the ac⁴C peaks that were present in both the respective hemizygous double mutant and the wild type, 144 and 179 transcripts differed by at least a log₂ fold change of ± 2 in *acyr1 acyr2/+* versus Col-0 and *acyr1/+ acyr2* versus Col-0, respectively (Supplemental Fig. S13). A total of 114 transcripts fulfilling this criterion were identical in both comparisons. These data together indicate that there is a significant functional overlap between ACYR1 and ACYR2 (Supplemental Figs. S12 and S13).

We compared the distribution of ac⁴C peaks along protein-coding transcripts relative to gene features, using a single splice variant for each gene. The location of peak center points was used to assign each ac⁴C peak to 1 of 4 nonoverlapping regions: 5′-untranslated region (UTR), coding sequence (CDS), intron, and 3′-UTR. Most ac⁴C peaks were located in the CDS: 72.8% in Col-0 and even more (~85%) in the hemizygous ACYR double mutants because acetylation modifications in other regions were suppressed by lowering the ACYR gene dosage in the mutants (Fig. 7D). In Col-0, introns, which were occasionally present due to alternative splicing or sequencing of pre-mRNAs, were approximately ten times less acetylated than exon sequences when the data were normalized to the respective amounts of intron/exon sequence in the sample. A metaplot of ac⁴C peak distribution across the 5′-UTR, CDS, and 3′-UTR features of mRNAs confirmed that the ac⁴C modifications were more abundant in the CDS with a slight bias toward the 3′-region of the CDS (Fig. 7E). Notably, the ac⁴C distribution in *acyr1 acyr2/+* was similar to that in Col-0, whereas in *acyr1/+ acyr2*, the bias toward the 3′-region was not observed, maybe because ACYR2 is especially important for acetylation in that region of the CDS. Taken together, these data show that ACYR1 and ACYR2 preferentially acetylate the CDS in protein-coding transcripts.

To determine whether there are conserved motifs in the identified ac⁴C peaks, we performed an unbiased search in regions surrounding ac⁴C peak summits using the MEME (Multiple EM for Motif Elicitation) suite (Ma et al. 2014) (Fig. 7F and Supplemental Table S2). The most markedly enriched motif (approximately 50%) was a C-rich motif,

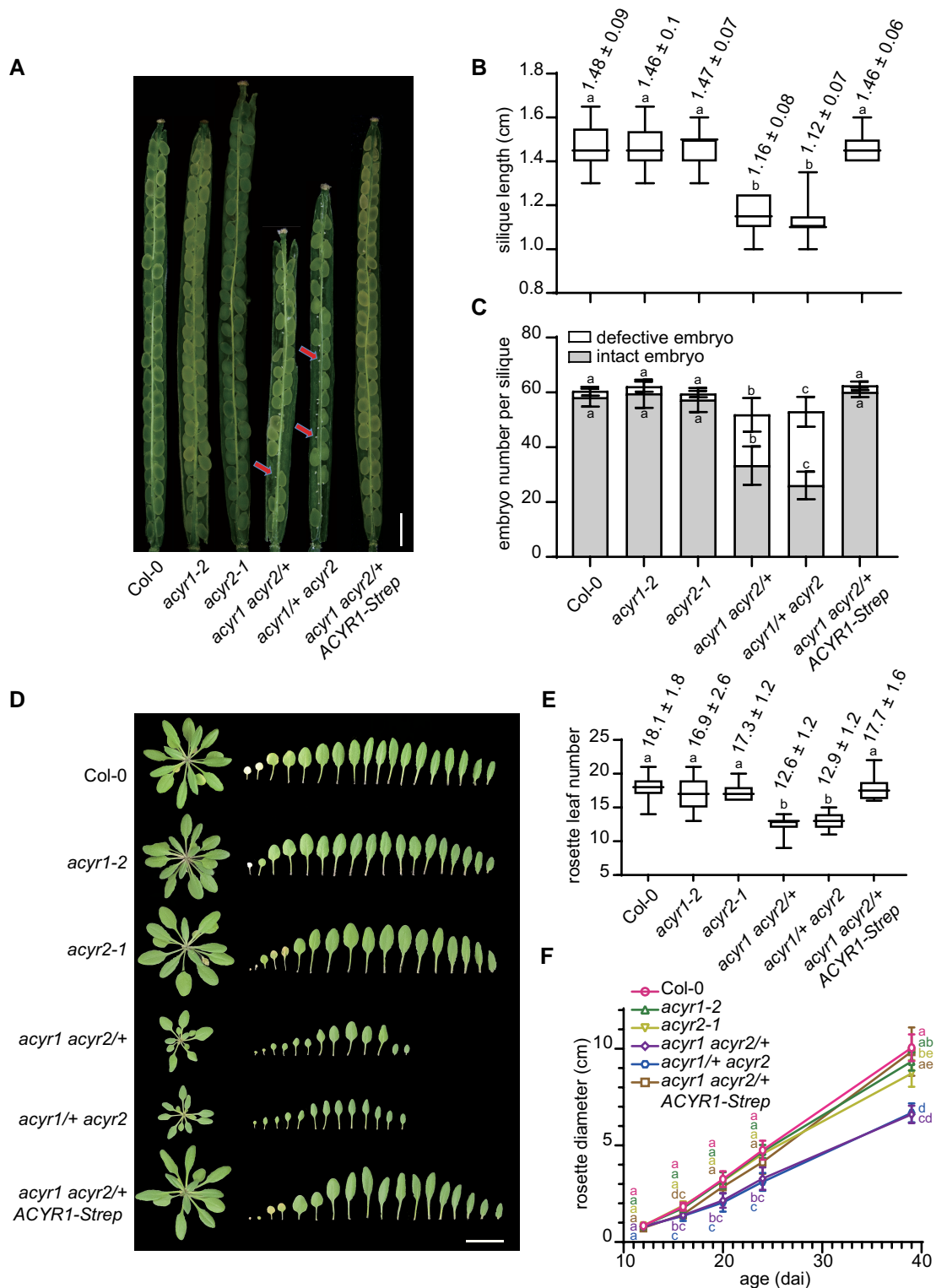


Figure 5. Loss of ACYR function suppresses seed development and vegetative growth. **A**) Developing seeds in the siliques of wild type, *acyr1-2*, *acyr2-1*, *acyr1 acyr2/+*, and *acyr1/+ acyr2* at 10 days after fertilization (DAF). Scale bar = 1 mm. Arrows indicate undeveloped embryos. **B**) Silique length of different genotypes at 10 DAF. Error bars are SD ($n = 20$ siliques from 5 independent plants for each genotype). In each boxplot, horizontal line, median; edges of boxes, 25th (bottom) and 75th (top) percentiles; whiskers, minimum and maximum silique length, respectively. The values of the mean and the SD are shown above each data display. Different letters indicate significant differences at $P < 0.05$ (one-way ANOVA along with two-sided Tukey's pairwise comparisons). **C**) Undeveloped and intact embryo number per silique of different genotypes. Error bars are SD ($n = 20$ siliques from 5 independent plants for each genotype). The values of the mean and the SD are shown above each data display.

(continued)

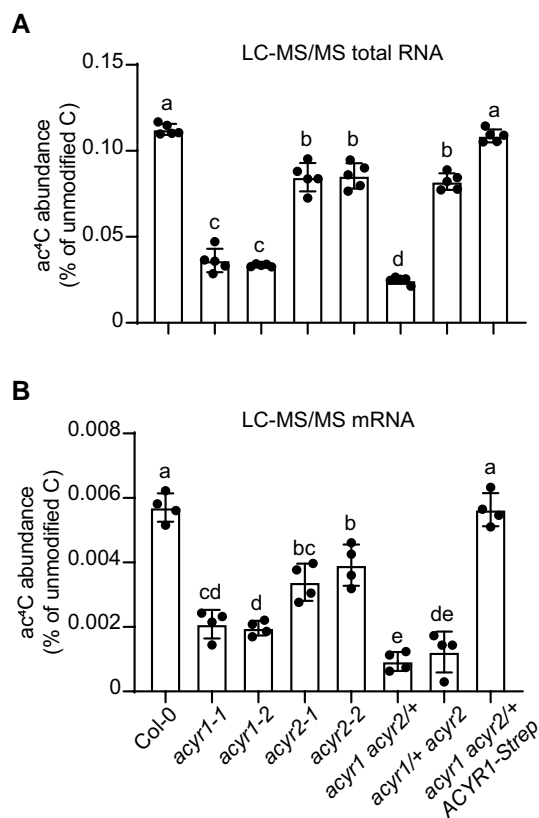


Figure 6. RNA acetylation by ACYR1 and ACYR2 in vivo. **A)** ac⁴C/C ratio in total RNA from 4-week-old rosette leaves of wild type, *acyr1-1*, *acyr1-2*, *acyr2-1*, *acyr2-2*, *acyr1 acyr2/+*, and *acyr1/+ acyr2* and the complementation line analyzed by LC-MS/MS. Error bars are SD ($n = 5$ biological replicates; biological replicates are parallel measurements of biological distinct samples). Different letters indicate significant differences at $P < 0.05$ (one-way ANOVA along with two-sided Tukey's pairwise comparisons). **B)** Same as in (A) but for mRNA. Error bars are SD ($n = 4$ biological replicates; biological replicates are parallel measurements of biological distinct samples).

CCWCCDCC (W = A or U or G; D = U or G or A), among confident ac⁴C peaks in Col-0 (Fig. 7F), resembling the conserved motif identified in mammalian cells (Arango et al. 2018).

ACYR-mediated ac⁴C modifications increase miRNA abundance by stabilizing *TGH* mRNA

To further investigate the molecular link between reduced ac⁴C modifications and the developmental alterations of

acyr1 acyr2/+ and *acyr1/+ acyr2* plants, we performed transcriptome deep sequencing (RNA-seq) of rosette leaves from 4-week-old Col-0 plants and the 2 hemizygous ACYR double mutants with 3 biological replicates each (Supplemental Data Set 3). To explore possible correlations between the RNA-seq data and acRIP-seq data, the log₂ fold changes of both parameters comparing Col-0 and *acyr1 acyr2/+* or *acyr1/+ acyr2* were plotted against each other for transcripts with a log₂ fold change of ± 0.2 (Fig. 8A, Supplemental Fig. S14, Supplemental Data Set 4). Compared to Col-0, we identified 67 transcripts in the *acyr1 acyr2/+* mutant with less ac⁴C modification, including 26 with increased (Fig. 8A, green) and 41 with decreased (Fig. 8A, blue) abundance. Likewise, we identified 59 transcripts with lower levels of ac⁴C modification, including 20 that were more abundant (Supplemental Fig. S14, green) and 39 that were less abundant (Supplemental Fig. S14, blue) in the *acyr1/+ acyr2* mutant relative to Col-0 (Supplemental Data Set 4).

Of the transcripts that were differentially acetylated and changed in abundance in the hemizygous double mutants versus Col-0, several were found in both hemizygous double mutant lines (Supplemental Fig. S15). Cytidine acetylation of the *TOUGH* transcript (*TGH*, At5g23080) was strongly reduced (Fig. 8B top panel), and its abundance was significantly reduced in both hemizygous ACYR double mutants relative to Col-0 (Supplemental Data Set 4). These results were also confirmed by acRIP-qPCR and RT-qPCR assays (Fig. 8B bottom panel and 8C). Transcription inhibition assays showed that the *TGH* transcript was less stable in the 2 hemizygous ACYR double mutants compared to Col-0 and the complementation line, whereas the stability of a nonacetylated control mRNA (*PLUTO*, At5g03555) was not influenced by the different genotypes (Fig. 9A). Notably, the stability of another ac⁴C-containing transcript (*S1P*, At5g19660) was also reduced in the 2 hemizygous ACYR double mutants compared to Col-0 and the complementation line, indicating that mRNA acetylation can apparently promote RNA stability.

The null mutation of *TGH* results in smaller plants with fewer rosette leaves in *Arabidopsis* (Calderon-Villalobos et al. 2005), which resembles the vegetative growth defects seen in both hemizygous ACYR double mutants. *TGH* functions in the early steps of miRNA biogenesis. Its mutation leads to the reduced accumulation of several miRNAs, including miR159, miR165/166, miR167, miR172, miR319, and miR390 (Ren et al. 2012). To assess whether the ACYR enzymes modulate vegetative growth by influencing miRNA

(Figure 5. Continued)

Different letters indicate significant differences at $P < 0.05$ (one-way ANOVA along with two-sided Tukey's pairwise comparisons). **D)** Rosettes and rosette leaves of the wild type, the ACYR single mutants, the 2 hemizygous ACYR double mutants, and the complementation line at 39 days after imbibition (dai). Bar = 5 cm. **E)** Number of rosette leaves of the different genotypes at 39 dai. In each boxplot, horizontal line, median; edges of boxes, 25th (bottom) and 75th (top) percentiles; whiskers, minimum and maximum leaf number, respectively. Error bars are SD ($n = 16$ independent plants). The values of the mean and the SD are shown above each data display. Different letters indicate significant differences at $P < 0.05$ (one-way ANOVA along with two-sided Tukey's pairwise comparisons). **F)** Rosette diameters of plants of different genotypes ($n = 10$ independent plants) grown 39 dai under long-day conditions. Error bars are SD. Different letters indicate significant differences at $P < 0.05$ (one-way ANOVA along with two-sided Tukey's pairwise comparisons).

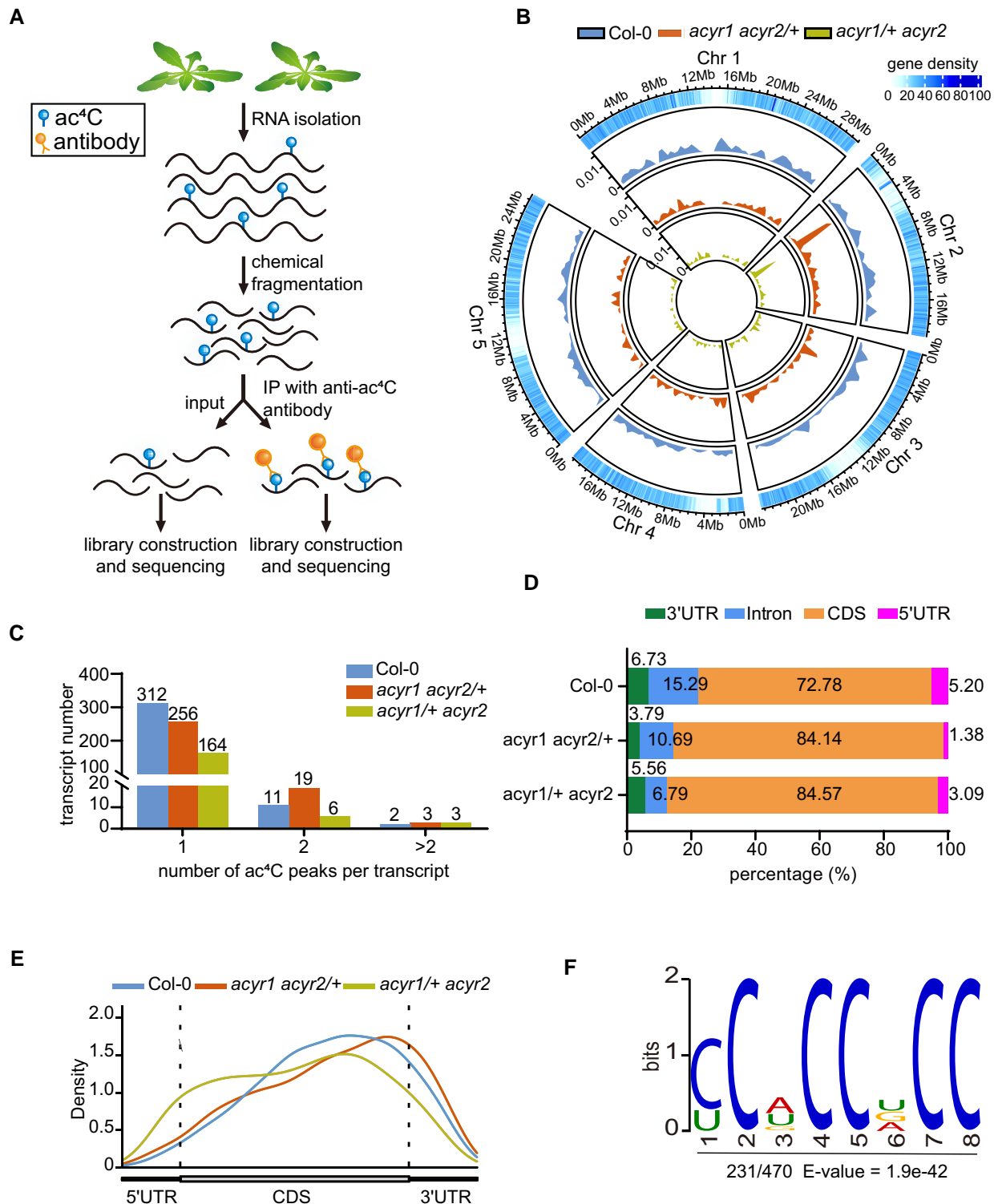


Figure 7. Transcriptome-wide mapping of ac⁴C in *Arabidopsis*. **A**) Scheme of the acRIP-seq procedure. Each genotype was performed with 2 biological replicates. Rosette leaves from 3 individual 4-week-old plants were pooled as 1 biological replicate. **B**) Circos plot of the ac⁴C peaks in the *Arabidopsis* genome. The 4 rings from the outside to the inside show (first) the genomic positions with gene density, (second) the ac⁴C peak density for Col-0, (third) for *acyr1 acyr2/+*, and (fourth) for *acyr1/+ acyr2*. Peak densities are drawn to the same scale. **C**) Numbers of transcripts bearing 1, 2, or >2 ac⁴C peaks. **D**) Bar chart presenting the distribution of ac⁴C peaks within 7 nonoverlapping segments of the protein-coding transcript in Col-0, *acyr1 acyr2/+*, and *acyr1/+ acyr2* lines. **E**) Metagene profile presenting the distributions of ac⁴C peaks identified in Col-0, *acyr1 acyr2/+*, and *acyr1/+ acyr2* lines across the indicated mRNA segments. **F**) Sequence logo representation of the consensus ac⁴C motif identified in Col-0 by MEME suite. The number of motif occurrences relative to the total number of ac⁴C peaks and the corresponding E-value are shown under the logo.

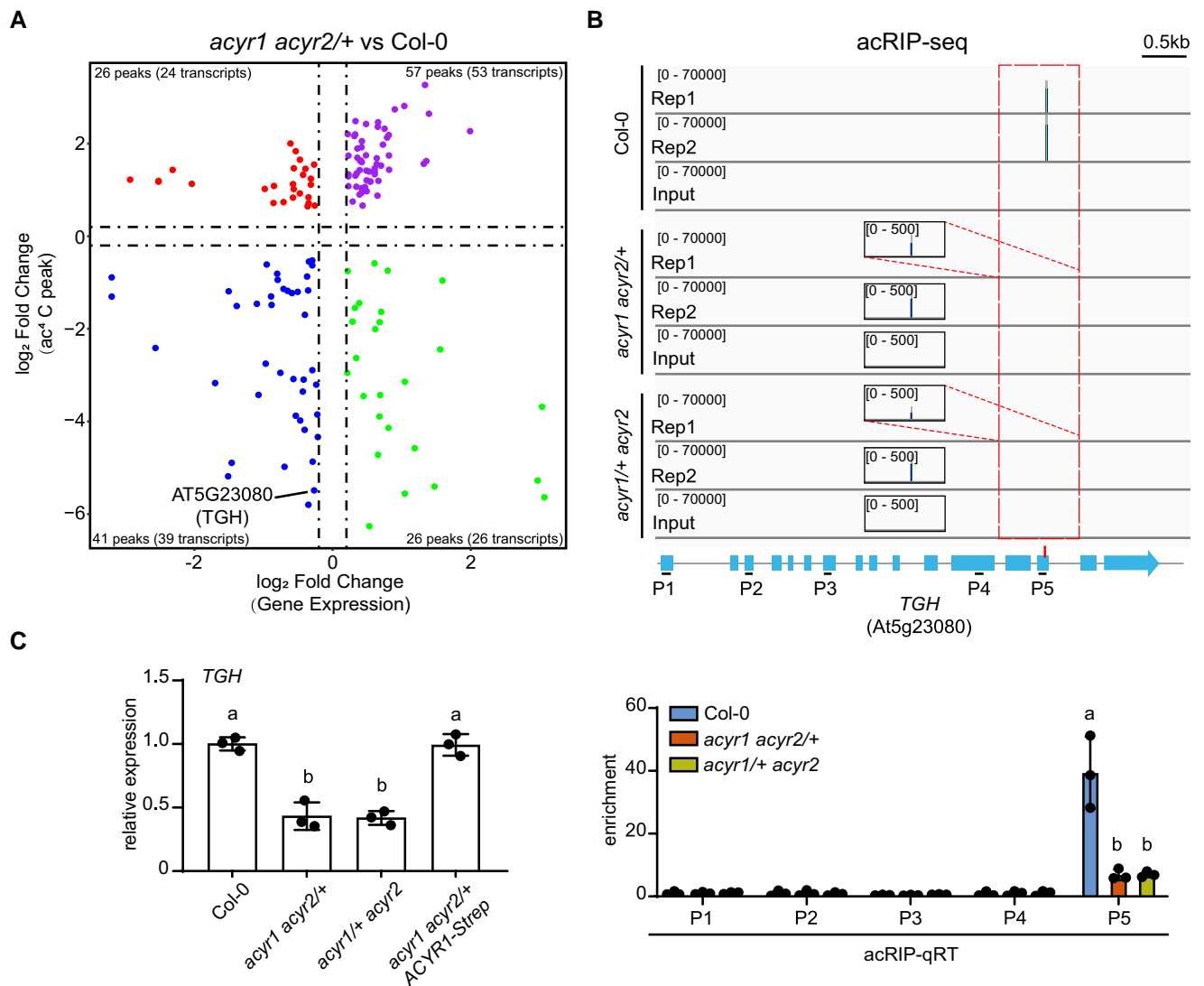


Figure 8. ACYR-mediated ac⁴C modifications enhance *TGH* transcript levels. **A**) Correlation between the level of gene expression and ac⁴C abundance in the *acyr1 acyr2/+* mutant compared to Col-0. $P_{adj} < 0.05$, log FC (fold change) > 0.2 or < -0.2 . The numbers of peaks and the associated transcripts are labeled in each quadrant. **B**) ac⁴C modification of the *TGH* transcript is reduced in both hemizygous ACYR double mutants. The top panel shows the ac⁴C density along the *TGH* transcript in ac⁴C-IP and input samples from Col-0 and the 2 hemizygous double mutants. The gene structure of *TGH* is displayed below the ac⁴C density maps, with exons depicted as blue boxes. The ac⁴C modification site is indicated on the gene structure. The bottom panel shows acRIP-qPCR results. Fragments amplified are indicated and numbered below the *TGH* gene structure. Different letters indicate significant differences at $P < 0.05$ (one-way ANOVA along with two-sided Tukey's pairwise comparisons). Error bars are SD ($n = 3$ biological replicates; biological replicates are parallel measurements of biological distinct samples). **C**) Relative *TGH* transcript levels in Col-0, the 2 hemizygous ACYR double mutants, and the complementation line determined by RT-qPCR. Error bars are SD ($n = 3$ biological replicates; biological replicates are parallel measurements of biological distinct samples). Different letters indicate significant differences at $P < 0.05$ (one-way ANOVA along with two-sided Tukey's pairwise comparisons).

production through the acetylation of *TGH* mRNA, we quantified several miRNAs in rosette leaves of 4-week-old Col-0, the 2 hemizygous ACYR double mutants, and the complementation line. Indeed, all miRNAs known to be dependent on TGH activity were less abundant in the 2 hemizygous ACYR double mutants compared to Col-0 and the complementation line (Fig. 9B).

In conclusion, these data show that ac⁴C modification prolongs the lifetime and thereby increases the abundance of

TGH transcripts. This promotes the formation of several miRNAs, which represent an important factor in vegetative development (Fig. 10).

Discussion

It has been noted that 18S rRNA of *Arabidopsis* and several other eukaryotes carries ac⁴C modifications (Sharma et al. 2015). However, while this modification in mRNA has been

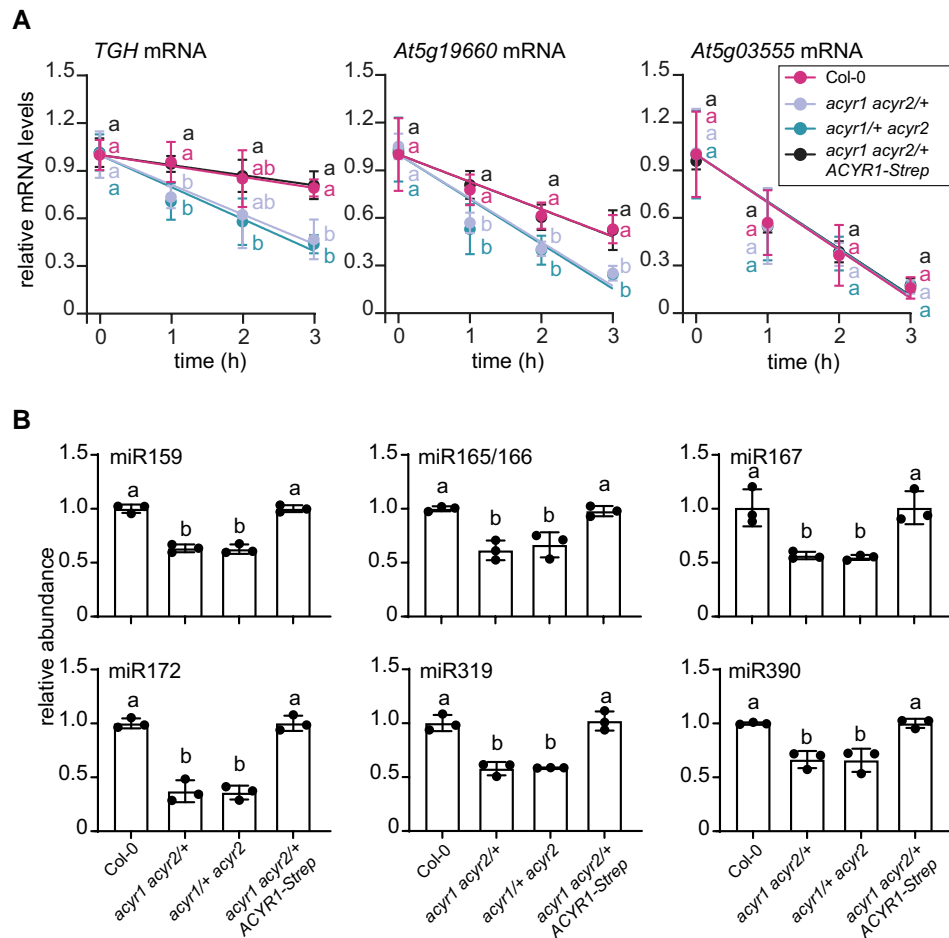


Figure 9. ac^4C modifications stabilize the *TGH* transcript and influence the amounts of several miRNAs. **A**) Transcript abundance (quantified by RT-qPCR) of *TGH*, and *SIP* (positive control) and *PLUTO* (negative control) in 20-day-old seedlings of Col-0, the hemizygous *ACYR* double mutants, and the complementation line when de novo transcription was blocked by treatment with actinomycin D for up to 3 h. Error bars are SD ($n = 3$ biological replicates * 2 technical replicates). Biological replicates are parallel treatments of biological distinct samples, and technical replicates are repeated measurements of the same sample. Different letters indicate significant differences at $P < 0.05$ (one-way ANOVA along with two-sided Tukey's pairwise comparisons). **B**) Relative abundances of miR159, miR165/166, miR167, miR172, miR319, and miR390 detected by RT-qPCR in 24-day-old seedlings of the wild type (Col-0), the 2 hemizygous mutants, and the complementation line. Error bars are SD ($n = 3$ biological replicates; biological replicates are parallel measurements of biological distinct samples). Different letters indicate significant differences at $P < 0.05$ (one-way ANOVA along with two-sided Tukey's pairwise comparisons).

described in mammals (Arango et al. 2018), little is known about its occurrence in the mRNA of other eukaryotes, including plants. Notably, the abundance and distribution of ac^4C modifications in plants are markedly different from those in mammalian cells. Here we found that in *Arabidopsis*, only $0.115 \pm 0.005\%$ and $0.004 \pm 0.0017\%$ cytidine nucleosides were N⁴-acetylated in total RNA and mRNA, respectively, which is far less than the $\sim 0.5\%$ and 0.2% in total RNA and mRNA of human cells, respectively (Arango et al. 2018). Compared to 4,250 ac^4C peaks identified in HeLa cells, we only mapped 470 ac^4C peaks associated with 325 transcripts in *Arabidopsis*. Additionally, we observed that ac^4C modifications are distributed along the CDS of the mRNAs, with some slight enrichment in the 3'-regions, whereas in HeLa cells, ac^4C was more abundant close to the 5'-region of the CDS, suggesting that the

biological function of ac^4C may differ between plants and mammals.

RNA methylation influences several RNA metabolic processes including splicing, stability, translocation, and translation (Gilbert et al. 2016; Yang et al. 2017; Frye et al. 2018). In mammalian cells, RNA acetylation increases RNA stability and stimulates translation efficiency (Arango et al. 2018). In plants, we showed that even partial reduction in ac^4C levels in certain target transcripts can significantly accelerate their degradation (Fig. 9A), suggesting that ac^4C modification could play a role in promoting mRNA stability. However, not always is a lower degree of C acetylation associated with lower transcript abundance—even the contrary can be true (Fig. 8, Supplemental Fig. S14). The molecular mechanisms behind such destabilizing or stabilizing functions remain unclear, but ac^4C reader proteins could be involved.

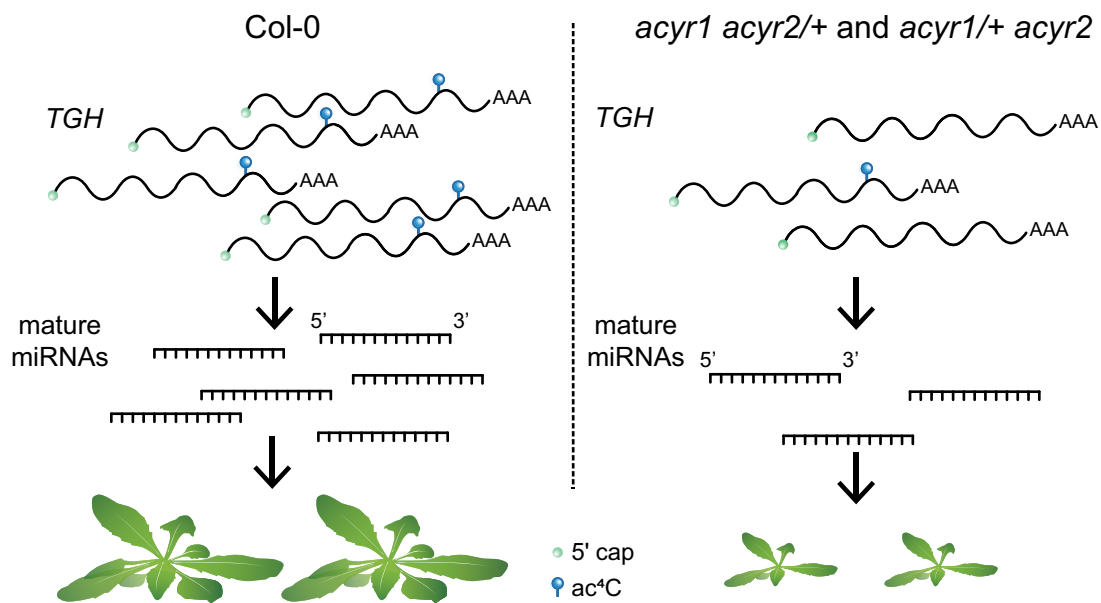


Figure 10. Proposed model showing how ACYR-dependent ac⁴C modification modulates vegetative growth through TGH-mediated miRNA processing. In the wild type of *Arabidopsis thaliana*, TGH transcripts are acetylated by ACYR proteins for promoting RNA stability, which is essential for miRNA homeostasis and vegetative growth. While in the *acyr1 acyr2/+* and *acyr1/+ acyr2* mutants, ac⁴C modification in TGH is highly reduced, leading to the decreased miRNA abundance and defects in leaf development.

If such readers exist, it would be interesting to identify them and elucidate how they work. In addition, it needs to be investigated whether ac⁴C in plant mRNAs influences translation or other process such as splicing and the nuclear export of RNA.

In plants, m⁶A is introduced by an evolutionarily conserved methyltransferase complex comprising 2 methyltransferases, mRNA adenosine methylase (MTA) and MTB, and several accessory subunits including FIP37, VIR, and HAKAI (Růžička et al. 2017; Shen 2023) and is dynamically removed by demethylase such as ALKBH10B (Duan et al. 2017) and ALKBH9B (Martínez-Pérez et al. 2017; Tang et al. 2022). Here, we showed that most ac⁴C modification sites in plant RNAs are installed by the mammalian NAT10 homologs ACYR1 and ACYR2. Interestingly, the mutation of *Arabidopsis* ACYRs did not completely eliminate ac⁴C modifications (Fig. 5B and C). This result can be explained either by the only partial loss of ACYR activity in our mutants or by the activity of some currently unknown cytidine acetyltransferases. The NAD-dependent protein deacetylase sirtuin-7 (SIRT7), 1 of the 7 mammalian sirtuins, was recently described as an rRNA deacetylase that directly interacts with NAT10 (Xu et al. 2021), indicating that ac⁴C modifications (such as m⁶A) are dynamic and could be regulated by writer and eraser proteins. However, whether *Arabidopsis* SRT1 (encoded by At5g55760) and SRT2 (encoded by At5g09230), 2 mammalian SIRT7 homologs, are the ac⁴C easers remains unknown.

NAT10/ACYR is a single-copy gene in many organisms, including most plants, but interestingly, there are 2 copies in the Brassicaceae and thus also in *Arabidopsis*. Sequence analysis suggested that both isogenes may have distinct functions in *Arabidopsis*, but functional analysis indicated that ACYR1 and ACYR2 are both required for full acetylation of coding and noncoding RNAs and have an overlapping substrate spectrum, although with different preferential substrates. Despite the apparent redundancy, it appears that the more abundant rRNAs are to a greater extent acetylated by ACYR1, explaining the stronger negative impact on the total acetylation level when ACYR1 was mutated. 18S rRNA is highly acetylated, which could explain why YFP-labeled ACYR enzymes accumulated in a nuclear subcompartment that might be the nucleolus (Fig. 3B).

Loss of function in either ACYR1 or ACYR2 reduced ac⁴C modification levels without affecting plant growth, while the complete loss of both ACYR1 and ACYR2 function in *Arabidopsis* led to embryonic lethality, pointing to the functional redundancy between ACYR1 and ACYR2. Similarly, homozygous *nat10* mutants are lethal before embryonic day E14.5 in mice (*Mus musculus*) (Balmus et al. 2018), indicating that ACYR-mediated ac⁴C modification plays an essential role in eukaryotic development.

The segregation ratios measured from the progeny of the hemizygous mutants suggest that both the female and the male gametophytes suffer when there is not enough cytidine-N-acetylation. If the *acyr1 acyr2* ovules died but

the corresponding double mutant pollen were viable, one would expect a 1:1:0 ratio of wild type/heterozygous/mutant genotypes for the respective hemizygous allele, and in the silique, ~0% of positions would be empty. When selfing the *acyr1 acyr2/+* hemizygous line, we observed a 1:1:0 ratio but only ~35% empty positions in the silique. This indicates that the *acyr1 acyr2* ovule suffers and many die but that some fertilized *acyr1 acyr2* ovules survive, and those that receive an ACYR2 (+) allele from the pollen can sometimes generate a viable seed. When the *acyr1/+ acyr2* hemizygous line was selfed, a 20:1:0 ratio with 50% empty siliques was observed, indicating that ACYR2 has a more important role for the gametes than ACYR1. It appears that pollen viability is also strongly compromised in plants in which the ACYR1 gene dosage is lowered in an *acyr2* null background, explaining the skewed allele frequency toward the wild type. The complete depletion of TGH in plants does not affect seed production (Calderon-Villalobos et al. 2005), indicating that the defective acetylation of transcripts other than TGH must be responsible for the observed partial infertility. The reduction of ac⁴C levels in nonpolyadenylated RNA in the 2 hemizygous ACYR double mutants may also contribute to the pleiotropic phenotypic alterations observed in these mutants.

This transcriptome-wide description of RNA ac⁴C modification in plants is only the tip of the iceberg. Investigating ac⁴C function in detail for individual transcripts will be possible by mutating the acetylation sites without affecting the coding potential in the case of mRNAs. It is likely that dynamic ac⁴C writing and perhaps erasing occur to transmit regulatory cues. It will be interesting to investigate whether additional regulatory components promote or prevent access of the ACYR proteins to their in vivo targets.

Materials and methods

Plant material and cultivation

The *Arabidopsis thaliana* ecotype Col-0 was chosen as the wild type. T-DNA insertion mutants of *Arabidopsis* from the SAIL collection (SAIL804E05, *acyr1-1*) (Sessions et al. 2002) and the SALK collection (SALK070262, *acyr1-2*; SALK011936, *acyr2-1*; and SALK110812, *acyr2-2*) (Alonso et al. 2003) were obtained from the Nottingham *Arabidopsis* Stock Centre. Hemizygous ACYR double mutants (*acyr1 acyr2/+* and *acyr1/+ acyr2*) were obtained by crossing *acyr1-2* (as the pollen donor) and *acyr2-1*. The T-DNA insertions were confirmed using the primer pairs 1197/Cp2, N61/Cp3, N61/Cp7, and N61/Cp8 for *acyr1-1*, *acyr1-2*, *acyr2-1*, and *acyr2-2*, respectively, and the primer pairs Cp1/Cp2, Cp3/Cp4, Cp7/Cp10, and Cp7/Cp10 for the wild-type alleles of *acyr1-1*, *acyr1-2*, *acyr2-1*, and *acyr2-2*, respectively (Supplemental Table S3).

Plants were cultivated on agar plates containing half-strength Murashige and Skoog (1/2 MS) medium or full nutrient soil under long-day conditions (16 h light of 75 $\mu\text{mol m}^{-2} \text{s}^{-1}$ intensity provided by white LED lamps at 22 °C

and 8 h dark at 20 °C, 75% relative humidity). For quantification of ACYR1 or ACYR2 expression, wild-type seedlings and apical meristems were sampled from 2-week-old plants, while rosette leaves, cauline leaves, stems, flowers, roots, and siliques were randomly collected from 6-week-old plants.

RNA extraction, reverse transcription, and quantitative RT-PCR analysis

Total RNA was isolated from different tissues or plants using TRIzol reagent (Monad) and treated with DNase (4 \times gDNA wiper mix; Vazyme Biotech Co. Ltd.), and cDNA was prepared using HiScript II Q Select RT Super Mix (Vazyme Biotech Co. Ltd.). Random primers were used for reverse transcription in the experiment evaluating rRNA contamination in mRNA, and oligo dT was used for the other experiments. Primer pairs Cp28/Cp29 and Cp32/Cp33 were employed for ACYR1 and ACYR2 cloning, introducing the NdeI/XmaI and XmaI/BamHI sites, respectively. The resulting PCR products were inserted into the vector pXNS1pat-YFP (V99) and pXNScpmv-HA-Strep (V89) (Chen and Witte 2020) for subcellular localization analyses and the generation of the complementation lines, respectively.

To analyze mRNA abundance, quantitative reverse transcription PCR (qRT-PCR) was performed with QuantStudio 1 (Thermo Fisher Scientific) using Hieff qPCR SYBR Green Master Mix (Yeasen Biotechnology) according to the manufacturer's instructions. Transcript abundance of ACYR1, ACYR2, TGH, SIP, PLUTO, and 18S rRNA was analyzed by employing the primer pairs Cp923/Cp924 or Cp175/Cp176, Cp198/Cp199 or Cp177/Cp178, Cp211/Cp212, Cp619/Cp620, Cp715/Cp716, and Cp448/Cp449, respectively. ACTIN2 was amplified with the primer pairs Cp204/Cp205 as an internal reference gene for quantifying rRNA contamination in mRNA, and the TIP41-like gene (Czechowski et al. 2005) was amplified with the primer pair Cp307/Cp308 as an internal reference gene for the transcript stability and other qRT-PCR analyses. The calculation was based on the $2^{-\Delta\Delta\text{CT}}$ method (Livak and Schmittgen 2001). To measure gene-specific mRNA levels in the mutants and the complementation line, cDNAs were prepared from seedlings of each genotype, and primer pairs Cp28/Cp29 and Cp32/Cp33 were used for the quantification of ACYR1 and ACYR2 transcripts.

To detect mature miRNAs, first-strand cDNA of individual miRNA was synthesized from 1 μg total RNA using an miRNA 1st Strand cDNA Synthesis Kit (by stem-loop; Vazyme Biotech Co. Ltd.) according to the manufacturer's instructions. Stem-loop RT primers were designed as described previously (Chen et al. 2005). Approximately 50 nM of TAFII15-StLp-cDNA_rv (Cp421) (Werner et al. 2021) was added as an internal control for qRT-PCR analysis, and 50 nM of the respective miRNA-specific stem-loop primer Cp479, Cp483, Cp487, Cp386, Cp489, or Cp491 was used for cDNA synthesis of miR159, miR165/166, miR167,

miR172, miR319, and miR390, respectively. A 5-fold dilution of cDNA was used for qRT-PCR. The primer pair Cp387/Cp478, Cp387/Cp482, Cp387/Cp486, Cp387/Cp390, Cp387/Cp488, or Cp387/Cp490 was employed in qRT-PCR analyses of mature miRNAs of miR159, miR165/166, miR167, miR172, miR319, or miR390, respectively. *TBP-ASSOCIATED FACTOR II 15 (TAFII15)* (Werner et al. 2021) amplified by primers Cp395/Cp396 was used as reference genes. The sequences of primers used in RT-qPCR analyses are listed in Supplemental Table S3.

To detect mRNA modifications, mRNA was isolated from total RNA for digestion using the PolyATtract mRNA Isolation Systems III (Promega). For mRNA preparation, 2 rounds of purification were performed. The RNA was quantified using a NanoDrop spectrophotometer (Thermo Scientific), and the purity and integrity of the RNA were assessed by applying 100 ng of RNA per sample on a Bioanalyzer 2100 system (Agilent).

Quantitative analyses of the ac⁴C/C ratio in RNA by LC-MS/MS

RNA samples were fully digested into single nucleosides as described previously (Chen et al. 2018; Chen and Witte 2020) with minor modifications. Approximately 800 ng of total RNA or mRNA isolated from 2-week-old seedlings of *Arabidopsis thaliana* (Col-0), *Zea mays* (Cultivar B73), *Solanum lycopersicum* (Micro-Tom), *Oryza sativa* (Nipponbare), *Nicotiana benthamiana*, and *Glycine max* (Williams 82) were individually digested by benzonase (0.4 unit; Sigma-Aldrich), phosphodiesterase I (0.004 units; Sigma-Aldrich), and shrimp alkaline phosphatase (0.04 unit; NEB) in 50 μ L of buffer containing 10 mM Tris-HCl, pH 7.9, 1 mM MgCl₂, and 0.1 mg mL⁻¹ BSA. After incubation at 37 °C for 10 h, the samples were filtered in ultrafiltration tubes (3 kDa cutoff; Pall), and 2 μ L aliquots were analyzed by an Agilent 1290 HPLC system coupled to a Sciex 6500 Qtrap mass spectrometer. The nucleosides were separated on a WATERS T3 column (2.1 \times 100 mm; particle size 1.8 μ m) at a flow rate of 0.3 mL min⁻¹. Solvent A was 0.1% formic acid, and Solvent B was acetonitrile. The gradient was 0 min, 5% B; 0.5 min, 5% B; 3 min, 90% B; 4 min, 90% B; 4.1 min, 5% B and 7 min, 5% B. The mass transitions *m/z* 286.3 to 112 for N⁴-acetylcytidine and *m/z* 244.3 to 111.9 for cytidine were monitored. Standard solutions of cytidine (1, 5, 25, 50, 100, 200, 400, 2,000, and 10,000 ng mL⁻¹) and N⁴-acetylcytidine (0.005, 0.01, 0.05, 0.1, 0.5, 1, 5, 25, and 50 ng mL⁻¹) were used for quantification. The ratio of N⁴-acetylcytidine to cytidine was calculated based on the calibrated concentrations.

Subcellular localization and immunoblot analysis

YFP-ACYR1 or YFP-ACYR2 was transiently coexpressed with the nucleus marker protein RFP-H2B (CFP fused to histone 2B) (Martin et al. 2009) in *N. benthamiana* leaves for 5 d. The samples were analyzed using a ZEISS LSM 980 with Airyscan2 microscope equipped with an HC PLAPO CS2

40 \times 1.0 water immersion objective (ZEISS Microsystems). The acquired images were processed using ZEN 2.3 (blue edition) software (Carl Zeiss Microscopy GmbH).

Monoclonal anti-Strep antibody from mouse (1:1000; Abcam, ab184224) was used together with antimouse IgG conjugated to horseradish peroxidase (HRP; 1:1000; Solarbio SE131) to detect Strep on immunoblots employing a WesternBright™ ECL kit (Advansta, Lot: 220616-60).

Analysis of transcript stability

For the transcription inhibition assays, 20-day-old seedlings of the wild type (Col-0), *acyr1 acyr2/+*, or *acyr1/+ acyr2* mutants were transferred to a 1/2 mS medium containing 100 μ M actinomycin D (AbMole BioScience). Six seedlings of each genotype were collected at 0, 1, 2, and 3 h after treatment. Total RNA was then extracted for reverse transcription and quantification of gene expression levels. 18S rRNA was used as an internal reference gene.

RNA-seq

Triplicate biological replicates of total RNA were isolated from 4-week seedlings of wild type (Col-0), *acyr1 acyr2/+*, and *acyr1/+ acyr2* mutants as described above. Rosette leaves from 3 individual plants were pooled as 1 biological replicate. The purity and integrity of the RNA were assessed by a NanoDrop spectrophotometer (Thermo Scientific) and a Bioanalyzer 2100 system (Agilent). mRNA was isolated from total RNA as described above. A total amount of 1 μ g RNA per sample was applied as input material for RNA sample preparation. The RNA library was generated by Novogene Co. Ltd. using a NEBNext Ultra™ RNA Library Prep Kit for Illumina (NEB) following the manufacturer's recommendations, and index codes were added to attribute sequences to each sample. Transcriptome sequencing (RNA-seq) was performed on an Illumina NovaSeq platform. Clean data (clean reads) were obtained by removing reads containing adapter, reads containing ploy-N, and low-quality reads from raw data (raw reads). The resulting reads were aligned to the *Arabidopsis* reference genome (TAIR10) using Hisat2 v2.0.5 (Mortazavi et al. 2008). The mapped reads of each sample were assembled by StringTie (v1.3.3b) (Pertea et al. 2015) using a reference-based approach. FeatureCounts v1.5.0-p3 was used to calculate FPKM of each gene (Liao et al. 2014). Differential expression analysis was performed using the DESeq2 R package (1.20.0) (Love et al. 2014). Genes with an adjusted *P*-value <0.05 were assigned as differentially expressed.

acRIP-seq and validation

The acRIP-seq analyses were performed by DIATRE Biotechnology, Shanghai, China, according to a previous description (Arango et al. 2018) with minor modifications. Briefly, total RNA was extracted from the tissues and treated with DNase as described above. The amount and quality of RNA were tested using gel electrophoresis, an Equalbit RNA BR Assay Kit (Vazyme Biotech Co. Ltd.), and an Agilent Bioanalyzer 2100 system. Total RNA samples were

fragmented into ~150 nt using NEBNext Magnesium RNA Fragmentation buffer. Fragmented RNAs were incubated with 5 μ g anti-ac⁴C antibody (Abcam, ab252215) for 2 h at 4 °C in 100 μ l IP buffer containing PBS, 0.1% BSA, Triton X-100, and 40 U RNase inhibitor (NEB). The mixture was immunoprecipitated by incubation with Dynabeads Protein A for Immunoprecipitation (Thermo Fisher Scientific) at 4 °C for 2 h. After washing 5 times with IP buffer, the eluted RNA was precipitated by ethanol and used for library construction using a NEBNext Ultra™ RNA Library Prep Kit for Illumina (NEB). Sequencing was performed on an Illumina NovaSeq platform. Each genotype was performed with 2 biological replicates. Rosette leaves from 3 individual 4-week-old plants were pooled as 1 biological replicate for total RNA extraction.

acRIP-qRT-PCR was performed to validate the ac⁴C sequencing results. Immunoprecipitated RNA described as above was reverse transcribed with random hexamers using HiScript II Q Select RT Super Mix (Vazyme Biotech Co. Ltd.). Relative enrichment of the fragments within the target gene was determined by qRT-PCR and calculated by normalizing the amount of the fragment against that of the *TIP41-like* gene as an internal control and then by normalizing the value for the immunoprecipitated sample against that for the input. The primer pairs Cp702/Cp703, Cp704/Cp705, Cp706/Cp707, Cp708/Cp709, and Cp691/Cp692 were used to amplify fragments No. 1 to 5 of the *TGH* transcript, respectively.

Peak calling and analyses

Adaptors and low-quality reads were trimmed from raw sequencing reads with trim galore v0.6.6 using default parameters, and the resulting clean reads were mapped to the reference genome (TAIR10.51) using STAR (Dobin et al. 2013). Samtools (Li et al. 2009) were used to sort the SAM files. Peak calling was performed using MACS2 software with default settings (q value <0.05 and fold change >1). Based on the peak center position, peaks were assigned to 5'UTR, CDS, introns, and 3'UTR regions. The distribution of ac⁴C peaks along mRNAs was analyzed using guitar scripts (Cui et al. 2016). Consensus motifs containing ac⁴C peaks were identified by MEME-CHIP (Ma et al. 2014).

Phylogenetic analysis

Protein sequences for NAT10 were obtained from 46 plant species and 13 nonplant organisms (accession numbers in Supplemental Data Set 1). A phylogenetic tree was constructed with Mega X (Kumar et al. 2018) using the neighbor-joining method (Saitou and Nei 1987). A total of 1,000 bootstraps were performed. The alignment and tree files are provided in Supplemental File S1 and Supplemental File S2, respectively.

Statistical analysis

Statistical analysis was performed as previously described (Heinemann et al. 2021). R software (version 4.2.1) was

used with the CRAN packages multcomp and sandwich to perform two-sided Tukey's pairwise comparisons. Heteroscedasticity of the data set was examined using the sandwich variance estimator (Herberich et al. 2010; Pallmann and Hothorn 2016). Different letters indicate significant differences at $P < 0.05$. The adjusted P -values of the individual data sets are listed in Supplemental Data Set 5.

Accession numbers

The materials generated in this work are available on reasonable request from the authors. Sequence data related to this article can be found in the *Arabidopsis* information portal (<https://www.arabidopsis.org/>) under accession numbers ACYR1 (At1g10490), ACYR2 (AT3G57940), TGH (AT5G23080), S1P (At5g19660), PLUTO (At5g03555), SRT1 (At5g55760), SRT2 (At5g09230), ACTIN2 (At3g18780), TAFII15 (At4g31720), and TIP41-like (At4g34270). acRIP-seq and RNA-seq data in this study have been deposited in the National Center for Biotechnology Information Sequence Read Archive under BioProject PRJNA929652 and PRJNA930058, respectively.

Acknowledgments

The authors thank Jialei Wang for her help with mass spectrometry analyses, Christel Schmiechen for her assistance with seedling phenotype analyses, and Markus Niehaus for his help with statistical analyses. This work was financially supported by the Fundamental Research Funds for the Central Universities [grant number YDZX2023013]; the National Natural Science Foundation of China [grant number 31900907]; the Natural Science Foundation of Jiangsu Province, China [grant number BK20190528]; the International Centre for Genetic Engineering and Biotechnology [grant number CRP/CHN20-04_EC]; the Deutsche Forschungsgemeinschaft (DFG) [grant numbers CH2292/1-1 to M.C. and C.-P.W, WI3411/8-1, and INST 187/741-1 FUGG to C.-P.W.]; the Special Fund on Technology Innovation of Carbon Dioxide Peaking and Carbon Neutrality of Jiangsu Province [grant number BE2022306 to J.Y.]; and the start-up fund for advanced talents from Nanjing Agricultural University to M.C.

Author contributions

M.C. conceived the research. W.W., H.L., F.W., X.L., Y.S., J.Z., C.Z., L.G., and J.Y. performed the experiments. C.-P.W. and M.C. analyzed the data and wrote the manuscript. All authors read and agreed with the manuscript.

Supplemental data

The following materials are available in the online version of this article.

Supplemental Figure S1. The purity of the mRNA preparation.

Supplemental Figure S2. Identification of ac⁴C modification in total RNA and mRNA of *Arabidopsis* by mass spectrometry.

Supplemental Figure S3. Quantification of ac⁴C and m³U in total RNA and mRNA.

Supplemental Figure S4. Multiple alignment of 2 ACYRs from *Arabidopsis* and NAT10 from human.

Supplemental Figure S5. Characterization of mutants in ACYR1 or ACYR2.

Supplemental Figure S6. Expression analysis of ACYR1 and ACYR2 in seedlings of Col-0 and both hemizygous mutant lines.

Supplemental Figure S7. Characterization of the complementation line.

Supplemental Figure S8. Vegetative growth of the *acyr* lines.

Supplemental Figure S9. Pearson correlation analyses of acRIP-seq data from the wild type and the 2 hemizygous mutants.

Supplemental Figure S10. Uniquely and repeatedly identified ac⁴C-modified transcripts in the 2 replicates performed for each genotype in the acRIP-seq analysis.

Supplemental Figure S11. GO analysis of the ac⁴C containing transcripts in Col-0.

Supplemental Figure S12. Different and identical ac⁴C peaks identified in *acyr1 acyr2/+* versus Col-0 compared to *acyr1/+ acyr2* versus Col-0.

Supplemental Figure S13. Venn diagram for different ac⁴C-modified transcripts identified between *acyr1 acyr2/+* versus Col-0 and *acyr1/+ acyr2* versus Col-0.

Supplemental Figure S14. Correlation between differential gene expression and ac⁴C modification level in the *acyr1/+ acyr2* mutant compared to Col-0.

Supplemental Figure S15. Venn diagrams for the transcripts with differential abundance and ac⁴C modification level between *acyr1 acyr2/+* versus Col-0 and *acyr1/+ acyr2* versus Col-0.

Supplemental Table S1. Quantification of silique length and embryo number in wild type and mutants varying in ACYR expression

Supplemental Table S2. The most abundant consensus motif in Col-0, *acyr1 acyr2/+*, and *acyr1/+ acyr2* lines using MEME suite.

Supplemental Table S3. Primers used in this study.

Supplemental Data Set 1. NAT10 homologs from 46 plant species and 13 nonplant organisms

Supplemental Data Set 2. Confident ac⁴C peaks in Col-0, *acyr1 acyr2/+*, and *acyr1/+ acyr2*.

Supplemental Data Set 3. RNA-seq raw data overview.

Supplemental Data Set 4. Differential ac⁴C peaks in *acyr1 acyr2/+* versus Col-0, and *acyr1/+ acyr2* versus Col-0.

Supplemental Data Set 5. Adjusted *P*-values for all multiple comparisons.

Supplemental File S1. Sequence alignments of NAT10 homologs from 46 plant species and 13 nonplant organisms.

Supplemental File S2. Machine-readable tree file.

Conflict of interest statement. None declared.

References

- Alonso JM, Stepanova AN, Leisse TJ, Kim CJ, Chen HM, Shinn P, Stevenson DK, Zimmerman J, Barajas P, Cheuk R, et al. Genome-wide insertional mutagenesis of *Arabidopsis thaliana*. *Science*. 2003;301(5633):653–657. <https://doi.org/10.1126/science.1086391>
- Arango D, Sturgill D, Alhusaini N, Dillman AA, Sweet TJ, Hanson G, Hosogane M, Sinclair WR, Nanan KK, Mandler MD, et al. Acetylation of cytidine in mRNA promotes translation efficiency. *Cell*. 2018;175(7):1872–1886.e24. <https://doi.org/10.1016/j.cell.2018.10.030>
- Arango D, Sturgill D, Yang R, Kanai T, Bauer P, Roy J, Wang Z, Hosogane M, Schiffers S, Oberdoerffer S. Direct epitranscriptomic regulation of mammalian translation initiation through N4-acetylcytidine. *Mol. Cell*. 2022;82(15):2797–2814.e11. <https://doi.org/10.1016/j.molcel.2022.05.016>
- Balmus G, Larrieu D, Barros AC, Collins C, Abrudan M, Demir M, Geisler NJ, Lelliott CJ, White JK, Karp NA, et al. Targeting of NAT10 enhances healthspan in a mouse model of human accelerated aging syndrome. *Nat Commun*. 2018;9(1):1700. <https://doi.org/10.1038/s41467-018-03770-3>
- Calderon-Villalobos LIA, Kuhnle C, Dohmann EMN, Li H, Bevan M, Schwechheimer C. The evolutionarily conserved TOUGH protein is required for proper development of *Arabidopsis thaliana*. *Plant Cell*. 2005;17(9):2473–2485. <https://doi.org/10.1105/tpc.105.031302>
- Chen C, Ridzon DA, Broomer AJ, Zhou Z, Lee DH, Nguyen JT, Barbis M, Xu NL, Mahuvakar VR, Andersen MR, et al. Real-time quantification of microRNAs by stem-loop RT-PCR. *Nucleic Acids Res*. 2005;33(20):e179. <https://doi.org/10.1093/nar/gni178>
- Chen M, Urs MJ, Sánchez-González I, Olayioye MA, Herde M, Witte C-P. M⁶a RNA degradation products are catabolized by an evolutionarily conserved N6-methyl-AMP deaminase in plant and mammalian cells. *Plant Cell*. 2018;30(7):1511–1522. <https://doi.org/10.1105/tpc.18.00236>
- Chen M, Witte C-P. A kinase and a glycosylase catabolize pseudouridine in the peroxisome to prevent toxic pseudouridine monophosphate accumulation. *Plant cell*. 2020;32(3):722–739. <https://doi.org/10.1105/tpc.19.00639>
- Cui X, Wei Z, Zhang L, Liu H, Sun L, Zhang S-W, Huang Y, Meng J. Guita: an R/Bioconductor package for gene annotation guided transcriptomic analysis of RNA-related genomic features. *Biomed Res Int*. 2016;2016:8367534. <https://doi.org/10.1155/2016/8367534>
- Czechowski T, Stitt M, Altmann T, Udvardi MK, Scheible W-R. Genome-wide identification and testing of superior reference genes for transcript normalization in *Arabidopsis*. *Plant Physiol*. 2005;139(1):5–17. <https://doi.org/10.1104/pp.105.063743>
- Dobin A, Davis CA, Schlesinger F, Drenkow J, Zaleski C, Jha S, Batut P, Chaisson M, Gingeras TR. STAR: ultrafast universal RNA-Seq aligner. *Bioinformatics*. 2013;29(1):15–21. <https://doi.org/10.1093/bioinformatics/bts635>
- Dolata J, Taube M, Bajczyk M, Jarmolowski A, Szwejkowska-Kulinska Z, Bielewicz D. Regulation of plant microprocessor function in shaping microRNA landscape. *Front. Plant Sci*. 2018;9:753. <https://doi.org/10.3389/fpls.2018.00753>
- Duan H-C, Wei L-H, Zhang C, Wang Y, Chen L, Lu Z, Chen PR, He C, Jia G. ALKBH10B is an RNA N6-methyladenosine demethylase affecting *Arabidopsis* floral transition. *Plant Cell*. 2017;29(12):2995–3011. <https://doi.org/10.1105/tpc.16.00912>
- Frye M, Harada BT, Behm M, He C. RNA Modifications modulate gene expression during development. *Science*. 2018;361(6409):1346–1349. <https://doi.org/10.1126/science.aau1646>
- Frye M, Jaffrey SR, Pan T, Rechavi G, Suzuki T. RNA Modifications: what have we learned and where are we headed? *Nat Rev Genet*. 2016;17(6):365–372. <https://doi.org/10.1038/nrg.2016.47>
- Gilbert WV, Bell TA, Schaening C. Messenger RNA modifications: form, distribution, and function. *Science*. 2016;352(6292):1408–1412. <https://doi.org/10.1126/science.aad8711>

- Heinemann KJ, Yang S-Y, Straube H, Medina-Escobar N, Varbanova-Herde M, Herde M, Rhee S, Witte C-P. Initiation of cytosolic plant purine nucleotide catabolism involves a monospecific xanthosine monophosphate phosphatase. *Nature Commun.* 2021;12(1):6846. <https://doi.org/10.1038/s41467-021-27152-4>
- Herberich E, Sikorski J, Hothorn T. A robust procedure for comparing multiple means under heteroscedasticity in unbalanced designs. *PLoS One.* 2010;5(3):e9788. <https://doi.org/10.1371/journal.pone.0009788>
- Jones-Rhoades MW, Bartel DP, Bartel B. MicroRNAs and their regulatory roles in plants. *Annu Rev Plant Biol.* 2006;57(1):19–53. <https://doi.org/10.1146/annurev.arplant.57.032905.105218>
- Kumar S, Stecher G, Li M, Nkayaz C, Tamura K. MEGA X: molecular evolutionary genetics analysis across computing platforms. *Mol Biol Evol.* 2018;35(6):1547–1549. <https://doi.org/10.1093/molbev/msy096>
- Li H, Handsaker B, Wysoker A, Fennell T, Ruan J, Homer N, Marth G, Abecasis G, Durbin R. The sequence alignment/map format and SAMtools. *Bioinformatics.* 2009;25(16):2078–2079. <https://doi.org/10.1093/bioinformatics/btp352>
- Liao Y, Smyth GK, Shi W. Featurecounts: an efficient general purpose program for assigning sequence reads to genomic features. *Bioinformatics.* 2014;30(7):923–930. <https://doi.org/10.1093/bioinformatics/btt656>
- Livak KJ, Schmittgen TD. Analysis of relative gene expression data using real-time quantitative PCR and the $2^{-\Delta\Delta CT}$ method. *Methods.* 2001;25(4):402–408. <https://doi.org/10.1006/meth.2001.1262>
- Love MI, Huber W, Anders S. Moderated estimation of fold change and dispersion for RNA-Seq data with DESeq2. *Genome Biol.* 2014;15(12):550. <https://doi.org/10.1186/s13059-014-0550-8>
- Ma W, Noble WS, Bailey TL. Motif-based analysis of large nucleotide data sets using MEME-ChIP. *Nat Protoc.* 2014;9(6):1428–1450. <https://doi.org/10.1038/nprot.2014.083>
- Martin K, Kopperud K, Chakrabarty R, Banerjee R, Brooks R, Goodin MM. Transient expression in *Nicotiana benthamiana* fluorescent marker lines provides enhanced definition of protein localization, movement and interactions in planta. *Plant J.* 2009;59(1):150–162. <https://doi.org/10.1111/j.1365-313X.2009.03850.x>
- Martínez-Pérez M, Aparicio F, López-Gresa MP, Bellés JM, Sánchez-Navarro JA, Pallás V. Arabidopsis m⁶A demethylase activity modulates viral infection of a plant virus and the m⁶A abundance in its genomic RNAs. *Proc Natl Acad Sci U S A.* 2017;114(40):10755–10760. <https://doi.org/10.1073/pnas.1703139114>
- McCown PJ, Ruzskowska A, Kunkler CN, Breger K, Hulewicz JP, Wang MC, Springer NA, Brown JA. Naturally occurring modified ribonucleosides. *Wiley Interdiscip Rev RNA.* 2020;11(5):e1595. <https://doi.org/10.1002/wrna.1595>
- Mortazavi A, Williams BA, McCue K, Schaeffer L, Wold B. Mapping and quantifying mammalian transcriptomes by RNA-Seq. *Nat Methods.* 2008;5(7):621–628. <https://doi.org/10.1038/nmeth.1226>
- Pallmann P, Hothorn LA. Analysis of means: a generalized approach using R. *J Appl Stat.* 2016;43(8):1541–1560. <https://doi.org/10.1080/02664763.2015.1117584>
- Pertea M, Pertea GM, Antonescu CM, Chang T-C, Mendell JT, Salzberg SL. Stringtie enables improved reconstruction of a transcriptome from RNA-Seq reads. *Nat biotechnol.* 2015;33(3):290–295. <https://doi.org/10.1038/nbt.3122>
- Ren G, Xie M, Dou Y, Zhang S, Zhang C, Yu B. Regulation of miRNA abundance by RNA binding protein TOUGH in Arabidopsis. *Proc Natl Acad Sci U S A.* 2012;109(31):12817–12821. <https://doi.org/10.1073/pnas.1204915109>
- Růžička K, Zhang M, Campilho A, Bodi Z, Kashif M, Saleh M, Eeckhout D, El-Showk S, Li H, Zhong S, et al. Identification of factors required for m⁶A mRNA methylation in Arabidopsis reveals a role for the conserved E3 ubiquitin ligase HAKAI. *New Phytol.* 2017;215(1):157–172. <https://doi.org/10.1111/nph.14586>
- Saitou N, Nei M. The neighbor-joining method: a new method for reconstructing phylogenetic trees. *Mol Biol Evol.* 1987;4(4):406–425. <https://doi.org/10.1093/oxfordjournals.molbev.a040454>
- Samad AFA, Sajad M, Nazaruddin N, Fauzi IA, Murad AMA, Zainal Z, Ismail I. MicroRNA and transcription factor: key players in plant regulatory network. *Front Plant Sci.* 2017;8:565. <https://doi.org/10.3389/fpls.2017.00565>
- Sas-Chen A, Thomas JM, Matzov D, Taoka M, Nance KD, Nir R, Bryson KM, Shachar R, Liman GLS, Burkhart BW, et al. Dynamic RNA acetylation revealed by quantitative cross-evolutionary mapping. *Nature.* 2020;583(7817):638–643. <https://doi.org/10.1038/s41586-020-2418-2>
- Sessions A, Burke E, Presting G, Aux G, McElver J, Patton D, Dietrich B, Ho P, Bacwaden J, Ko C, et al. A high-throughput Arabidopsis reverse genetics system. *Plant Cell.* 2002;14(12):2985–2994. <https://doi.org/10.1105/tpc.004630>
- Sharma S, Langhendries J-L, Watzinger P, Kötter P, Entian K-D, Lafontaine DLJ. Yeast Kre33 and human NAT10 are conserved 18S rRNA cytosine acetyltransferases that modify tRNAs assisted by the adaptor Tan1/THUMP1. *Nucleic Acids Res.* 2015;43(4):2242–2258. <https://doi.org/10.1093/nar/gkv075>
- Shen L. Functional interdependence of m⁶A methyltransferase complex subunits in Arabidopsis. *Plant Cell.* 2023;35(6):1901–1916. <https://doi.org/10.1093/plcell/koad070>
- Shen L, Liang Z, Wong CE, Yu H. Messenger RNA modifications in plants. *Trends Plant Sci.* 2019;24(4):328–341. <https://doi.org/10.1016/j.tplants.2019.01.005>
- Tang J, Yang J, Lu Q, Tang Q, Chen S, Jia G. The RNA N⁶-methyladenosine demethylase ALKBH9B modulates ABA responses in Arabidopsis. *J Integr Plant Biol.* 2022;64(12):2361–2373. <https://doi.org/10.1111/jipb.13394>
- Voinnet O. Origin, biogenesis, and activity of plant microRNAs. *Cell.* 2009;136(4):669–687. <https://doi.org/10.1016/j.cell.2009.01.046>
- Werner S, Bartrina I, Schmölling T. Cytokinin regulates vegetative phase change in *Arabidopsis thaliana* through the miR172/TOE1-TOE2 module. *Nat Commun.* 2021;12(1):5816. <https://doi.org/10.1038/s41467-021-26088-z>
- Wiener D, Schwartz S. The epitranscriptome beyond m⁶A. *Nat Rev Genet.* 2021;22(2):119–131. <https://doi.org/10.1038/s41576-020-00295-8>
- Xu C, Zhang J, Zhang J, Liu B. SIRT7 is a deacetylase of N⁴-acetylcytidine on ribosomal RNA. *Genome Instab Dis.* 2021;2(4):253–260. <https://doi.org/10.1007/s42764-021-00046-x>
- Yang X, Yang Y, Sun B-F, Chen Y-S, Xu J-W, Lai W-Y, Li A, Wang X, Bhattarai DP, Xiao W, et al. 5-methylcytosine Promotes mRNA export-NSUN2 as the methyltransferase and ALYREF as an m⁵C reader. *Cell Res.* 2017;27(5):606–625. <https://doi.org/10.1038/cr.2017.55>
- Yu Y, Jia T, Chen X. The ‘how’ and ‘where’ of plant microRNAs. *New Phytol.* 2017;216(4):1002–1017. <https://doi.org/10.1111/nph.14834>
- Zhang Y, Liu T, Meyer CA, Eeckhoutte J, Johnson DS, Bernstein BE, Nusbaum C, Myers RM, Brown M, Li W, et al. Model-based analysis of ChIP-seq (MACS). *Genome Biol.* 2008;9(9):R137. <https://doi.org/10.1186/gb-2008-9-9-r137>